

## Process analysis and test of manufacturing of sleeve spring-type torsional vibration damper<sup>†</sup>

Beom Cheol Hwang<sup>1</sup>, Won Byong Bae<sup>2</sup> and Chul Kim<sup>1,\*</sup>

<sup>1</sup>Research Institute of Mechanical Technology, Pusan National University, Busan, 609-735, Korea

<sup>2</sup>School of Mechanical Engineering and RIMT, Pusan National University, Busan, 609-735, Korea

(Manuscript Received December 3, 2009; Revised February 25, 2010; Accepted March 25, 2010)

### Abstract

In diesel engines, engine torque fluctuation inevitably produces torsional vibration. A sleeve spring-type damper commonly is used to reduce this vibration. In this paper, closed form equations to predict the spring constant of a sleeve spring and the torsional characteristics of a torsional vibration damper are proposed for calculation of the stiffness of the damper. The equations were verified through finite element analysis (FEA) and experiments. In addition, the stability of the sleeve spring-type torsional vibration damper was verified in an analysis of the inner star and outer star (the core components of the damper). A two-roll bending process, proposed in this paper, was determined to be the most suitable for manufacture of the sleeve springs. A closed form equation to calculate the forming radius, taking account of the springback effect, was derived, and a FEA method used to analyze the elasto-plastic problem was verified through an analysis of a 90° bending process. The results of the analysis were in good agreement with the experiment. It is recommended that our proposed method, an advanced technique that can significantly reduce production costs, replace the conventional forming process.

**Keywords:** Sleeve spring; Spring constant; Torsional vibration damper; Two-roll bending

### 1. Introduction

Torsional vibration of a crankshaft due to variation of torque is inevitable in a diesel engine, which is a reciprocal engine with a crank mechanism. Such vibration can be reduced through installation of an appropriate damper or by optimization of the combustion chamber stroke. There are several types of torsional vibration dampers, and they are selected according to engine speed: a viscous fluid type for low speed, a coil spring type for medium speed, and a sleeve spring type for high speed. The sleeve spring torsional vibration damper is shown in Fig. 1, and the sleeve spring pack used in the MT881 Ka-500 Engine is shown in Fig. 2.

Chul Kim *et al.* [1] derived a spring constant formula for a sleeve spring and a torsional characteristic formula for a sleeve spring torsional vibration damper.

The techniques for the production of cylindrical tubular sections such as sleeve springs include roll-bending, stamp-bending, stretch-bending, and press-braking. Roll-bending, compared with the other processes, can reduce set up time, reduce costs in tooling investments, minimize the length of

straight end-edges remaining in finished products, and achieve much better finished dimensional accuracy and better circularity of cylindrical sections. Therefore, the roll-bending technique is widely used in forming products with cylindrical tubular sections. Various studies on three-roll bending [2-5] and four-roll bending [6-12] have been undertaken, but investigations into two-roll bending do not appear to be available in the literature. Roll bending is a complex process, and its forming mechanism is not yet fully understood. Many factors can influence the process: material properties, the geometry and configuration of the rolls, friction, temperature, and others.

In the present study, structural analyses of the inner star and the outer star, which are the core components of the torsional vibration damper, were performed, and a technique to manufacture a sleeve spring was studied, in order to develop a sleeve spring torsional vibration damper. The two-roll bending process is proposed here for the manufacture of the sleeve spring, because it is simpler than the three-roll and four-roll processes. Also, the two-roll bending process is mainly applied to the manufacture of small products, and therefore is more suitable for mass production than those other processes (three-roll bending and four-roll bending). We derived a closed-form equation to calculate the forming radius, taking account of the springback effect [13, 14], and we verified the FEA method used to analyze the elasto-plastic problem,

<sup>†</sup>This paper was recommended for publication in revised form by Associate Editor Chang-Wan Kim

\*Corresponding author. Tel.: +82 51 510 2489, Fax: +82 51 512 9835

E-mail address: chulkii@pusan.ac.kr

© KSME & Springer 2010

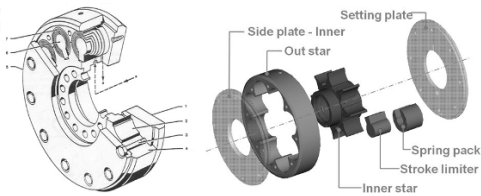


Fig. 1. Sleeve spring-type torsional vibration damper.

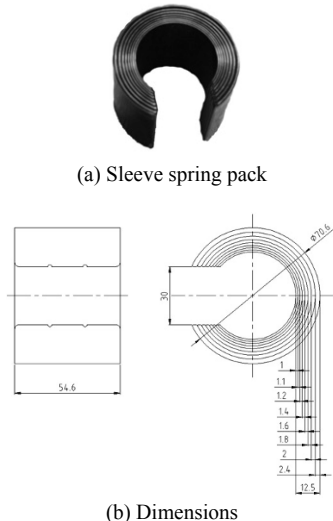


Fig. 2. Sleeve spring pack used in MT881 Ka-500 engine.

through an analysis of the 90°bending process. In addition, we conducted durability tests to verify the wear resistance of the inner star and the outer star according to heat treatment specifications.

## 2. Theory

### 2.1 Spring constant of sleeve spring and torsional characteristics of torsional vibration damper

The design parameters of the sleeve spring were determined as shown in Fig. 3. The spring constant of the sleeve spring is expressed as [1]

$$k = \frac{E \cdot h \cdot t^3}{12D \times \left[ \pi - \sin^{-1} \left( \frac{L_{GAP}}{D} \right) \right]}. \quad (1)$$

The dynamic characteristics of a torsional vibration damper can be conceived as functions of the torsional torque versus the torsional angle of the inner star. Fig. 4 shows the geometry of a sleeve spring, whether the inner star rotates or not, when a sleeve spring pack is assembled in the damper.

The relation between the angle of the open gap in the sleeve spring and the rotation angle of the inner star is expressed

$$\beta - \delta = \frac{(2\pi - \beta)R_{Pitch} \cdot \phi}{D_A - R_{Pitch} \cdot \phi}. \quad (2)$$

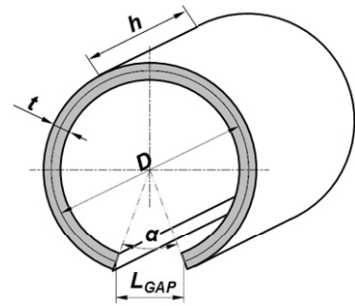


Fig. 3. Design parameters of sleeve spring.

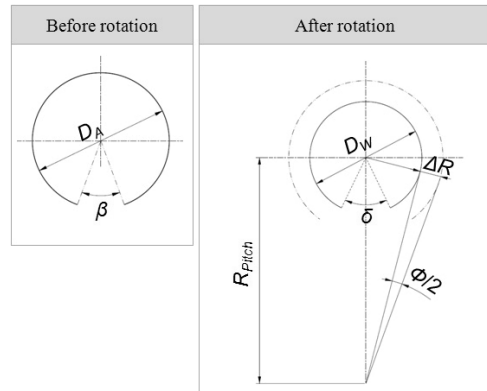


Fig. 4. Geometry of sleeve spring, whether inner star rotates or not.

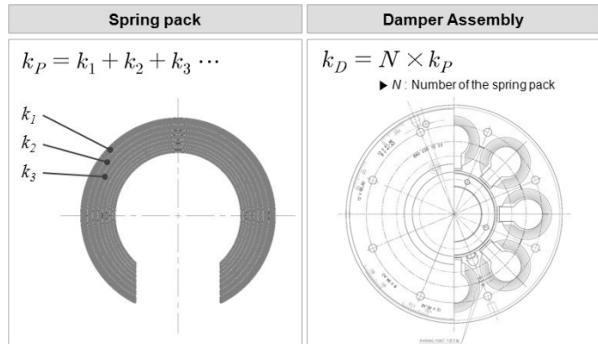


Fig. 5. Sleeve spring pack and damper assembly.

The sleeve spring pack used in the torsional vibration damper (Fig. 5) has a structure similar to leaf springs connected in parallel. The relation between the torsional torque and the rotation angle of the inner star of the torsional vibration damper is expressed as [1]

$$T = N_{SP} \times k_{SP} \times \frac{(2\pi - \beta)R_{Pitch} \cdot \phi}{D_A - R_{Pitch} \cdot \phi}. \quad (3)$$

### 2.2 Spring-back in the two-roll bending process

The coordinate system and nomenclatures describing the pure bending process are shown in Fig. 6. [13, 14] The bending moment needed to produce the bend results in stress in the X-direction, so the bending moment is expressed as

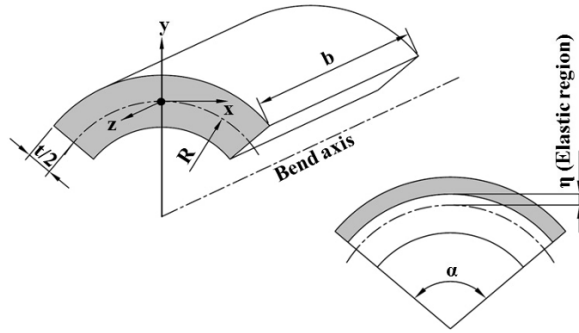


Fig. 6. Coordinate system and nomenclatures in pure bending process.

$$M = 2 \times \int_0^{t/2} \sigma_x \cdot (b \times dy) \cdot y . \quad (4)$$

Springback occurs upon removal of the bending moment. The subscript ‘i’ represents the values before springback and the subscript ‘f’ represents the values after springback. The stress deviation thus is expressed as

$$\Delta\sigma = E' \cdot \Delta\varepsilon = E' (\varepsilon_i - \varepsilon_f) = E' \left( \frac{y}{R_i} - \frac{y}{R_f} \right) \quad (5)$$

$$\text{where } E' = \frac{E}{1 - \nu^2} .$$

The deviation of the bending moment is expressed as

$$\Delta M = 2 \times \int_0^{t/2} \Delta\sigma \cdot (b \times dy) \cdot y = \frac{bt^3 E'}{12} \left( \frac{y}{R_i} - \frac{y}{R_f} \right) . \quad (6)$$

For nonlinear strain hardening material, flow stress, including the conditions of the plane-strain state and volume constancy is expressed as

$$\bar{\sigma} = K \cdot \left( \sqrt{\frac{4}{3}} \cdot \frac{y}{R_i} \right)^n . \quad (7)$$

After unloading, since the sum of the loading moment and unloading moment equals zero, we have

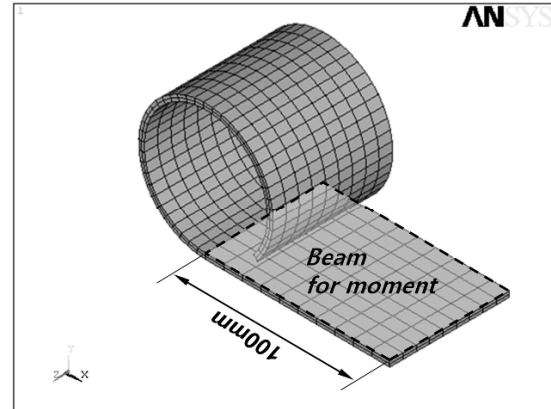
$$M - \Delta M = 0 . \quad (8)$$

Therefore, by Eqs. (4), (6) and (7), the relationship between the radii of the sleeve spring before and after springback is expressed as

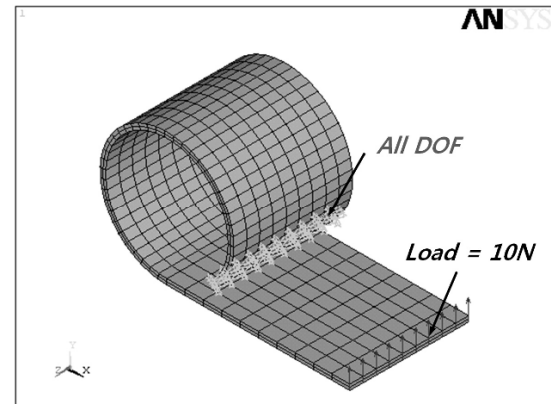
$$\frac{1}{R_i} - \frac{1}{R_f} = \frac{6}{n+2} \cdot \frac{1}{tE'} \cdot K \left( \frac{4}{3} \right)^{n/2} \cdot \left( \frac{t}{2R_i} \right)^n . \quad (9)$$

The forming radius is calculated by Eq. (10), which is converted from Eq. (9):

$$f(R_i) = \frac{6}{n+2} \cdot \frac{1}{tE'} \cdot K \left( \frac{4}{3} \right)^{n/2} \cdot \left( \frac{t}{2R_i} \right)^n - \frac{1}{R_i} + \frac{1}{R_f} = 0 . \quad (10)$$



(a) Modeling



(b) Boundary conditions

Fig. 7. Modeling and boundary conditions for obtaining spring constant of sleeve spring.

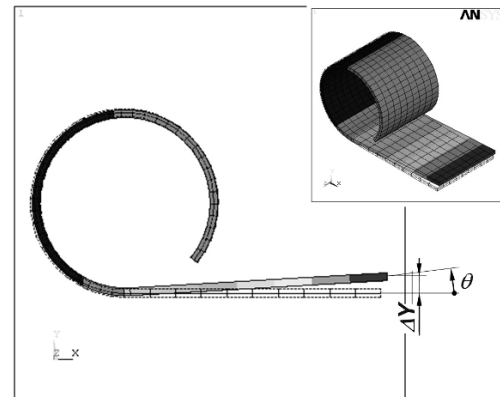


Fig. 8. Results obtained from finite element analysis (FEA).

### 3. Finite element analysis (FEA) and experiments on core components

#### 3.1 Sleeve spring

##### 3.1.1 Spring constant and torsional characteristics

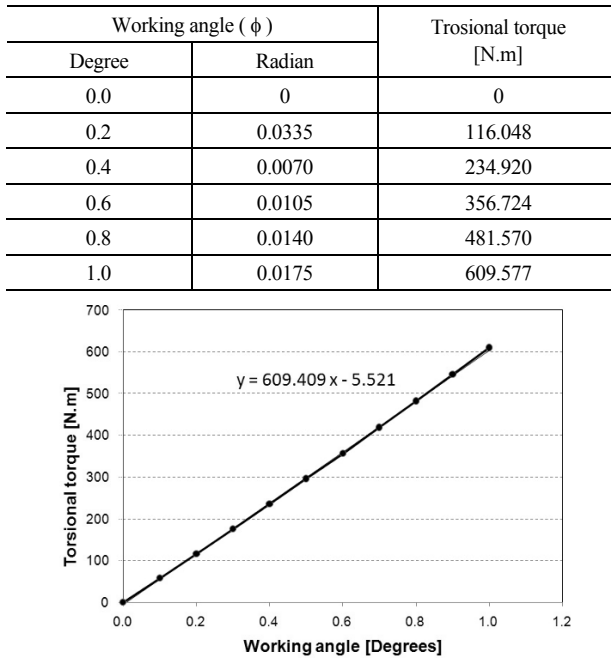
A finite element analysis (FEA) using Ansys® Version 11.0 was performed to verify the validity of the derived spring con-

Table 1. Comparison of spring constants between theoretical results and FEM results.

Thickness [mm]	Diameter [mm]	Spring constants [N.m/rad]		
		Equation	Analysis	Error ratio*
2.4	68.2	72.1031	72.1999	0.13
2.0	63.8	45.1770	45.6126	0.95
1.8	60.0	35.4755	35.9964	1.45
1.6	56.6	26.7706	27.2686	1.83
1.4	53.6	19.2010	19.6143	2.11
1.2	51.0	12.8843	13.1587	2.09
1.1	48.7	10.5388	10.8064	2.48
1.0	46.6	8.3959	8.5864	2.22
Spring Pack		230.5463	233.2433	1.16

\* (Analysis – Equation) / Analysis × 100%

Table 2. Torsional torque according to rotation angle of inner star.



stant. Fig. 7 shows the modeling and boundary conditions for obtaining spring constant of the sleeve spring. The spring constant was obtained by dividing the rotation angle into the applied moment. The rotation angle was obtained by converting deformation in the Y-direction, as shown in Fig. 8. Table 1 summarizes a comparison of theoretical results and the FEA results for the spring constants. [1]

The values of the theoretical results using the spring constant formula were always less than those of the FEM results, and the error between the theoretical results and the FEM was less than 2.48%, which indicated good agreement. The error between the theoretical results and the FEM for the spring pack was 1.16%. The torsional torque according to the rota-

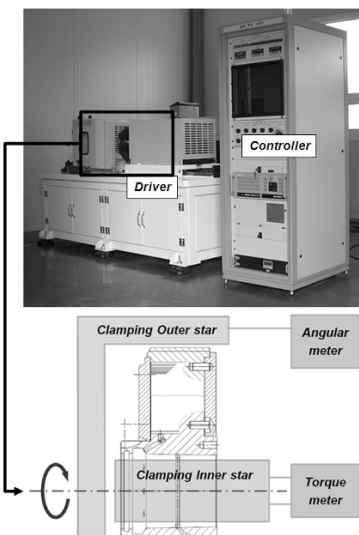


Fig. 9. Experimental equipment.

tion angle of the inner star was calculated by applying the values in Table 1 to Eq. (3), as shown in Table 2. In the result, the stiffness of the sleeve spring torsional vibration damper used in the MT881 Ka-550 engine was 609.4N.m/<sup>o</sup>.

### 3.1.2 Experimental equipment and performance test

Our test equipment comprised a driver, a controller, and a fan unit, as shown in Fig. 9. A torque meter was attached to the inner star component, and an angular meter was attached to the outer star component. The torsional torque and torsional angle were measured in real time during operation.

The experiment was carried out under the following conditions: velocity = 5cycle/sec, input torque = 1000N·m, number of cycles = 2000cycle. Fig. 10 shows the torsional torque and stiffness values according to the number of cycles. The performance test showed that abnormal values of torque were obtained until 1000 cycles, due to the low temperature of the oil, and that normal values of torque and stiffness were obtained after about 1500 cycles. The maximum values over all regions, and the average values over 30 data obtained between 1500 cycles and 2000 cycles, are shown in Table 3. Based on the values calculated using Eq. (3), the test samples were deemed to be within an error of 3%.

Therefore we could confirm that the stiffness coefficient theory for a sleeve spring applied to a sleeve spring torsional vibration damper was in good agreement with the test results.

### 3.1.3 Validation of finite element analysis (FEA) boundary conditions for two-roll bending

An FEA of the 90° bending process using DEFORM-2D Ver. 9.1 was performed to verify the validity of the boundary conditions in the elasto-plastic problem. Fig. 11 shows the die modeling for the 90° bending process. The punch, holder and die were assumed to be rigid bodies, and six layers of elements were used in the thickness direction. Fig. 12 shows the analysis procedures of the 90° bending process. First, the

Table 3. Experimental results via theoretical results.

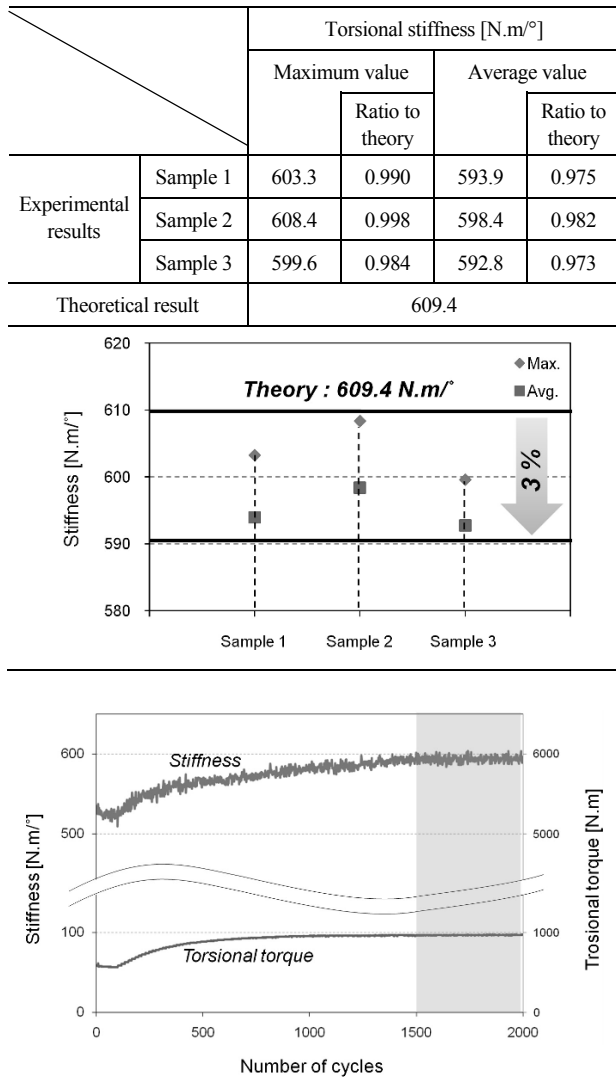


Fig. 10. Results of performance test.

punch moves downward to bend the material to  $90^{\circ}$ , and then the punch moves to the right until it is separated from the material.

Table 4 shows the analysis results according to the thickness. The results show an error of 3-6% compared with the design values.

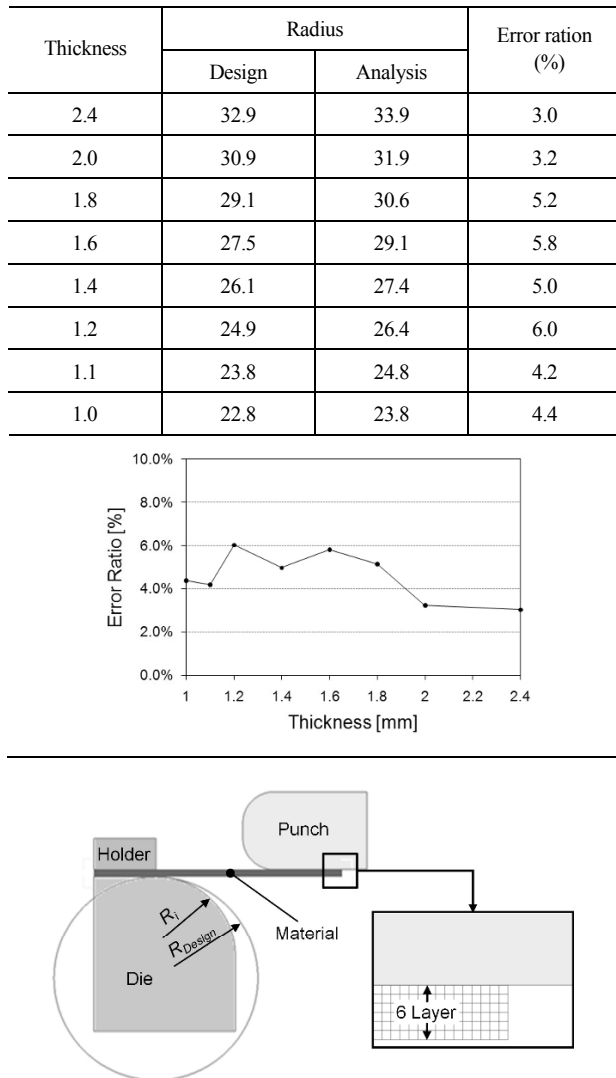
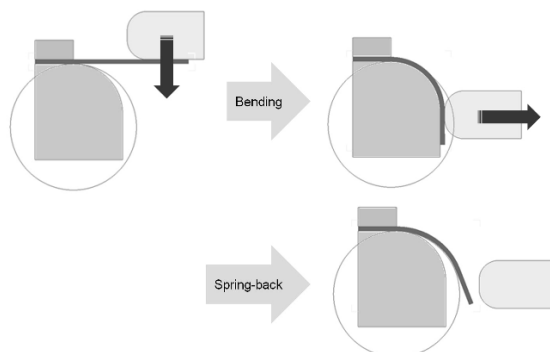
### 3.1.4 Finite element analysis (FEA) of two-roll bending

DEFORM-2D Ver. 9.1 was used for an FEA of the two-roll bending process. Fig. 13 shows the analysis model, which is based on a two-roll bending process used in the actual field. In the process, the bending roll is fixed, and a urethane-covered roll moves vertically while rotating.

However, in the analysis model, a urethane-covered roll with a deformed shape moved vertically to bend the material, and the bending roll rotated.

The main process parameters of two-roll bending are the material thickness, the diameter of the bending roll, and the

Table 4. Comparison between design values and analysis results.

Fig. 11. Die modeling for  $90^{\circ}$  bending process.Fig. 12. Analysis procedures of  $90^{\circ}$  bending process.

compressed amount of urethane-covered roll. The material thickness is determined based on the design value, and the diameter of the bending roll is determined by theoretical analysis.

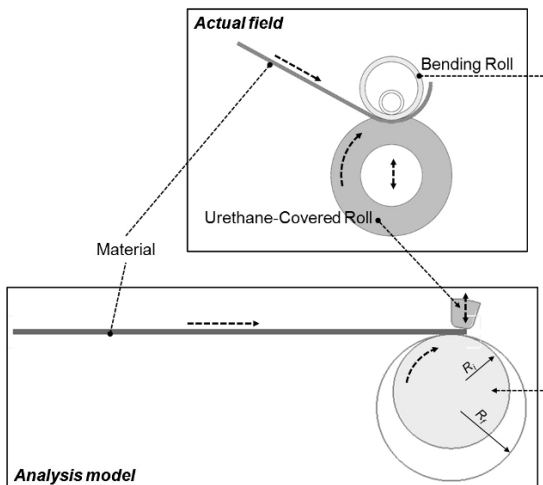


Fig. 13. Analysis model representing 2-roll bending process in actual field.

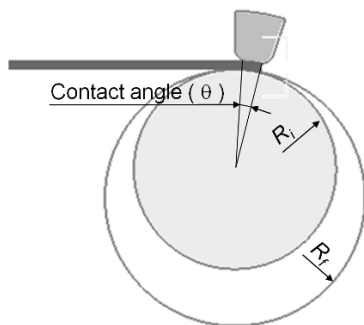


Fig. 14. Contact angle between bending roll and sheet.

Therefore only the compressed deformation of the urethane-covered roll needs to be determined. To that end, analyses according to the contact angle between the bending roll and the sheet were performed. This contact angle is illustrated in Fig. 14.

The analysis results for the contact angle between the bending roll and the sheet are listed in Table 5, and the errors of the analysis values compared with the design values are shown in Fig. 15.

### 3.1.5 Analysis results and discussion

The curves for the error ratio of analysis values to design values show different patterns, as indicated in Fig. 15. Therefore, a new process parameter incorporating the main process parameters (contact angle, material thickness, and forming radius) needs to be defined so that the curves for the error ratio of analysis values to design values regarding the various material thicknesses could have similar patterns without regard to those material thicknesses. Thus, in the present study, the new process parameter,  $\theta / (t \times R_i)$ , was defined. The values of the new process parameter are listed in Table 6.

The error ratios between the analysis values and design values versus the new process parameter,  $\theta / (t \times R_i)$ ,

Table 5. Analysis results of 2-roll bending process.

Contact Angle [°]	Thickness [mm]						
	2.4	2.0	1.8	1.6	1.4	1.2	1.0
10	31.43	28.80	-	-	-	-	-
9	31.96	28.90	27.27	-	-	-	-
8	33.58	29.10	27.67	25.78	-	-	-
7	33.62	30.05	27.79	25.88	24.24	-	-
6	35.69	30.69	28.43	26.13	24.54	23.40	-
5	41.04	32.96	30.05	27.00	24.72	23.69	-
4	-	-	-	28.08	25.08	23.61	21.79
3	-	-	-	-	26.81	24.35	21.90
2	-	-	-	-	-	25.10	22.44
1	-	-	-	-	-	-	22.80
0.5	-	-	-	-	-	-	23.18

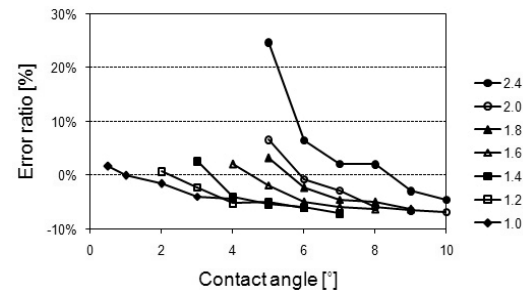


Fig. 15. Error ratios of analysis values to design values.

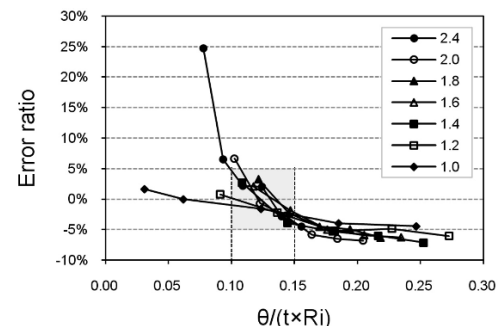


Fig. 16. Error ratios of analysis values to design values.

rial thickness  $\times$  forming radius), showed similar patterns, as indicated in Fig. 16. Therefore, in two-roll bending, the contact angle must be determined as the new process parameter has a constant value. In the case of 50CrV4, the value of the new process parameter is in the range of 0.1-0.15, and the error is within -5%-5% without regard to the material thickness and the forming radius.

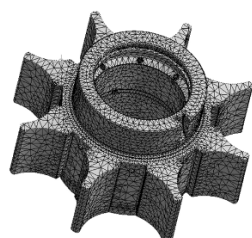
### 3.2 Inner star and outer star

#### 3.2.1 Finite element analysis (FEA)

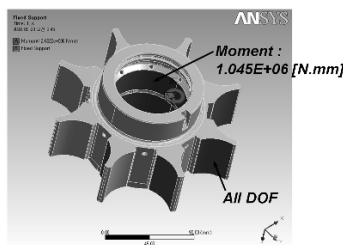
Ansys® 11.0 Workbench was used in an FEA of the inner

Table 6.  $\theta / (t \times R_i)$  converted from contact angle.

Contact Angle [°]	Thickness [mm]						
	2.4	2.0	1.8	1.6	1.4	1.2	1.0
10	0.155	0.205	-	-	-	-	-
9	0.140	0.184	0.218	-	-	-	-
8	0.124	0.164	0.194	0.235	-	-	-
7	0.109	0.143	0.170	0.205	0.253	-	-
6	0.093	0.123	0.146	0.176	0.217	0.273	-
5	0.078	0.102	0.123	0.147	0.180	0.227	-
4	-	-	-	0.117	0.144	0.182	0.247
3	-	-	-	-	0.108	0.136	0.185
2	-	-	-	-	-	0.091	0.123
1	-	-	-	-	-	-	0.062
0.5	-	-	-	-	-	-	0.031

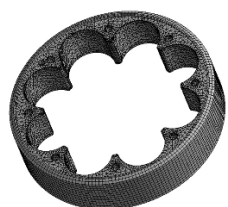


(a) Mesh

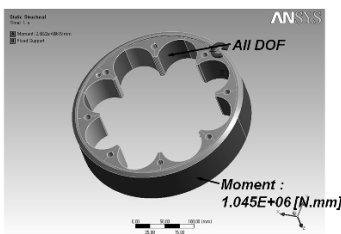


(b) Boundary conditions

Fig. 17. Modeling details and boundary conditions for structural analysis of inner star.



(a) Mesh



(b) Boundary conditions

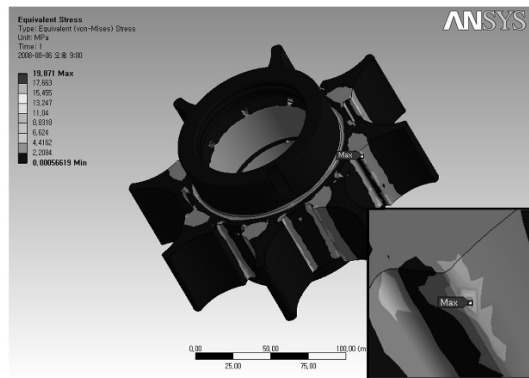
Fig. 18. Modeling details and boundary conditions for structural analysis of outer star.

star and the outer star. The maximum torsional torque exerted on the inner star and outer star occurred when the sleeve spring was compressed to its maximum. The elements and boundary conditions for the model of the inner star are shown in Fig. 17, and the elements and boundary conditions for the model of the outer star are shown in Fig. 18. Fig. 19 shows analysis results for the inner star and the outer star for an applied maximum torsional torque of  $1.048E+03$ N-m.

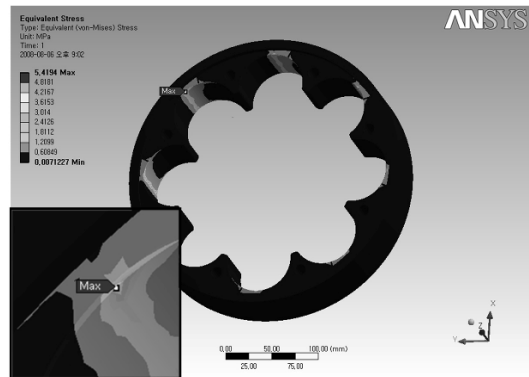
The maximum stresses of the inner star and the outer star were 19.9MPa and 5.4MPa respectively, which were below the tensile strength of the material (Min. 1000MPa for SNCM439). Thus, the structure did not appear to be subject to fatigue failure due to repeated loads on the inner star and the

Table 7. Heat treatment specifications of test samples.

Sample	Inner star		Outer star
	QT	High-frequency	QT
1	○	○	○
2	○	×	○
3	×	×	×



(a) Inner star



(b) Outer star

Fig. 19. Results obtained by structural analysis of inner star and outer star.

outer star.

### 3.2.2 Durability test

According to FEA results, fatigue failure due to repeated loads on the inner star and the outer star did not occur. So, durability tests were carried out to verify the wear resistance of the inner star and the outer star according to heat treatment specifications. Table 7 provides the test sample heat treatment specifications.

The experiments were carried out under the following conditions: velocity = 5cycle/sec, input torque = 1000N-m, number of cycles =  $10E+07$ cycle.

### 3.2.3 Durability test results and discussions

Fig. 20 shows the inner star according to the pertinent heat treatment specifications for the durability test. The wear pat-

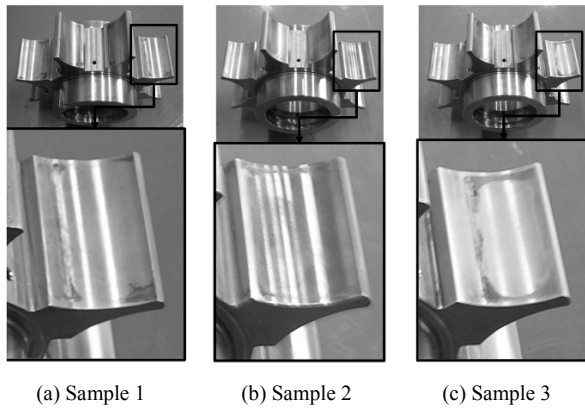


Fig. 20. Inner star after durability test.

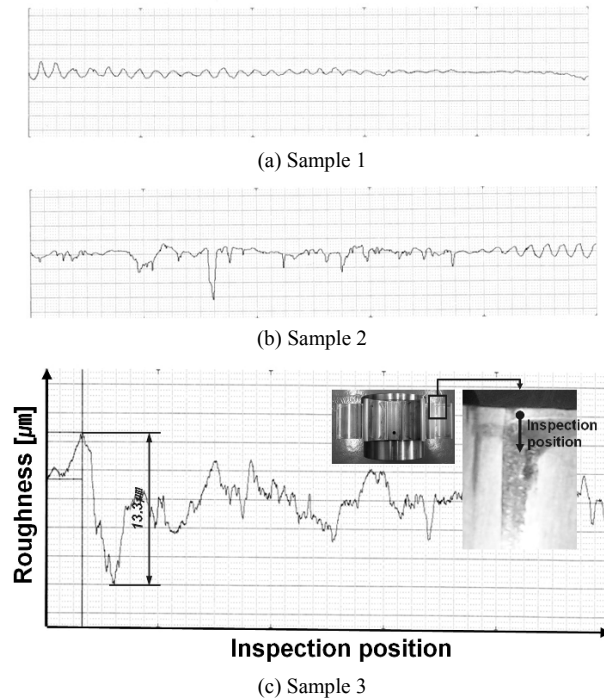


Fig. 21. Abrasion amount by durability test.

terns on the region contacting the sleeve spring were similar irrespective of the heat treatment specifications.

Fig. 21 shows the results of the measurement of the amount of wear using a roughness measuring instrument. Wear did not occur in sample 1. In sample 2, slight wear occurred. In sample 3 (no heat treatment applied), the amount of wear was about  $13.3\mu\text{m}$ . These results showed that quenching-tempering and high-frequency heat treatment must be applied to the inner start in order to prevent wear.

#### 4. Conclusions

A finite element analysis (FEA) of and experiments on the core components of a sleeve spring torsional vibration damper

were performed in this study. The key results obtained from this study are summarized as follows:

The spring constant formula of a sleeve spring was verified through performance tests.

The suitability of the FEA method for two-roll bending was confirmed. A new process parameter,  $[\text{contact angle} / (\text{material thickness} \times \text{forming radius})]$ , was tested, this parameter allows for the curves of the error ratios of analysis values to design values regarding the various material thicknesses to have similar patterns without regard to the material thicknesses.

To improve wear resistance, quenching-tempering and high-frequency heat treatment should be applied to the inner star, and quenching-tempering should be applied to the outer star.

#### Acknowledgment

This study was financially supported by Pusan National University in program Post-Doc. 2010 and the outcome of a Manpower Development Program for Energy & Resources supported by the Ministry of Knowledge and Economy (MKE).

#### Nomenclature

$D$	: Mean diameter
$D_A$	: Mean diameter in the damper
$E$	: Elastic modulus
$h$	: Height of the spring pack
$k$	: Spring constant
$k_{SP}$	: Spring constant of a sleeve spring pack
$L_{GAP}$	: Length of the open gap
$N_{SP}$	: Number of sleeve spring packs
$R_{Pitch}$	: Pitch radius of spring pack
$t$	: Thickness
$\beta$	: Angle of the open gap in the damper
$\delta$	: Angle of the open gap in the sleeve spring due to rotation of the inner star
$\phi$	: Rotation angle of the inner star
$\nu$	: Poisson's ratio

#### References

- [1] B. C. Hwang, C. Kim and W. B. Bae, A Study of Structural Analysis and Torsional Characteristic of the Sleeve Spring-Type Torsional Vibration Damper, *Korean Society for Precision Engineering*, 26 (2) (2009) 94-100.
- [2] M. Yang and S. Shima, Simulation of Pyramid Type Three-roll Bending Process, *International Journal of Mechanical Sciences*, 30 (12) (1988) 877-886.
- [3] G. Yang, K. Mori and K. Osakada, Determination of Forming Path in Three-Roll Bending Using FEM Simulation and Fuzzy Reasoning, *Journal of Material Processing Technology*, 45 (1994) 161-166.
- [4] W. Hu and Z. R. Wang, Theoretical Analysis and Experimental Study to Support the Development of a More Valuable Roll-bending Process, *International Journal of Machine*

*Tools and Manufacture*, 41 (2001) 731-747.

- [5] J. Zeng and Z. Liu, H. Champliaud, FEM dynamic simulation and analysis of the roll-bending process for forming a conical tube, *Journal of Material Processing Technology*, 198 (2008) 330-343.
- [6] M. Hua, D. H. Sansome, K. P. Rao and K. Baines, Continuous Four-roll Plate Bending Process: Its Bending Mechanism and Influential Parameters, *Journal of Material Processing Technology*, 45 (1994) 181-186.
- [7] M. Hua, K. Baines and I. M. Cole, Bending Mechanisms, Experimental Techniques and Preliminary Tests for the Continuous Four-Roll Plate Bending Process, *Journal of Material Processing Technology*, 48 (1995) 159-172.
- [8] M. Hua, I. M. Cole , K. Baines and K. P. Rao, A Formulation for Determining the Single-pass Mechanics of the Continuous Four-roll Thin Plate Bending Process, *Journal of Material Processing Technology*, 67 (1997) 189-194.
- [9] M. Hua and Y. H. Lin, Large Deflection Analysis of Elasto-plastic Plate in Steday Continuous Four-Roll Bending Process, *International Journal of Mechanical Sciences*, 41 (1999) 1461-1483.
- [10] M. Hua and Y. H. Lin, Effect of strain hardening on the Continuous Four-roll Plate Edge Bending Process, *Journal of Material Processing Technology*, 89-90 (1999) 12-18.
- [11] Y. H. Lin and M. Hua, Influence of strain hardening on Continuous Plate Roll-bending Process, *International Journal of Non-linear Mechanics*, 35 (2000) 883-896.
- [12] M. Hua, K. Baines and I. M. Cole, Continuous four-roll plate bending: a production process for the manufacture of single seamed tubes of large and medium diameters, *International Journal of Machine Tools and Manufacture*, 39 (1999) 905-935.
- [13] K. Lange, *Handbook of Metal Forming*, McGraw-Hill, New York, USA, (1985).
- [14] E. M. Melnik, *Metalworking Science Engineering*, McGraw-Hill, New York, USA, (1991).



**Beom-Cheol Hwang** received his B.S. degree in Mechanical Engineering from Pusan National University, Korea, in 1998. He received his M.S. and Ph.D. degrees in 2000 and 2010. Dr. Hwang is currently a Post-Doc. at the Research Institute of Mechanical Technology at Pusan National University in Busan, Korea. His research fields extend into machine component design, process planning, die design, CAD/CAM, and FEM simulation in the metal forming processes.



**Won-Byong Bae** received his B.S. degree in Mechanical Engineering from Sungkyunkwan University, Korea, in 1976. He received his M.S. and Ph.D. degrees from Korea Advanced Institute of Science and Technology in 1978 and 1992. Professor Bae is currently a Professor in the Department of Mechanical Engineering at Pusan National University in Busan, Korea. His research fields extend into machine component design, CAD/CAM, and FEM simulation in the metal forming processes.



**Chul Kim** received his B.S. degree in Mechanical Engineering from Pusan National University, Korea, in 1985. He received his M.S. and Ph.D. degrees in 1987 and 1997. Professor Kim is currently a Professor in the Research Institute of Mechanical Technology at Pusan National University in Busan, Korea. His research fields extend into process planning, die design, CAD/CAM, and FEM simulation in the metal forming processes.